CSCE 2022 Annual Conference
Whistler, British Columbia
May 25th – 28th, 2022

Reliability Based Optimal Design of Magnetic Negative Stiffness Damper Based Inerter for Efficient Energy Harvesting

Das, Sourav[1] and Tesfamariam, Solomon[2]
[1] Ph.D. Student, School of Engineering, The University of British Columbia, Okanagan Campus, Kelowna BC V1V 1V7, Canada
[2] Professor, School of Engineering, The University of British Columbia, Okanagan Campus, Kelowna BC V1V 1V7, Canada
[1] corresponding author: sds2019@mail.ubc.ca

Abstract: This study proposes a magnetic negative stiffness damper based inerter (MNSDI) for mitigating wind induced vibration of tall structures and energy harvesting. The proposed control system has a nonlinear magnetic negative stiffness damper which does not add any additional stiffness into the combined system by which the adjoining members of the proposed control system do not experience any additional force demand. Due to the movement of the magnets inside a conductive pipe, MNSDI introduces eddy current damping into the structural system. An electromagnetic transducer is attached to MNSDI to convert vibrational energy to electrical energy. As the proposed system is a passive damper, the design parameters related to the damper are needed to estimate before installation. In this context, a reliability-based design optimization (RBDO) is used to estimate the design parameters of MNSDI so that maximum energy harvesting can be achieved. As the RBDO framework is computationally expensive, Kriging is used as a surrogate model. For the numerical demonstration, a 76-storeys high-rise benchmark building is considered. The stationary wind loads are used where fluctuating components of wind loads are simulated from the Davenport spectrum. The numerical results show the effectiveness of the proposed control system to reduce the structural vibration as well as enhance its energy harvesting capability simultaneously.

Keywords: Inerter, Negative Stiffness, Energy Harvesting, Reliability-Based Optimization, Stationary Wind

1 Introduction

Due to the development of technology, civil engineering structures have become slenderer and are more prone to excessive vibration due to dynamic loads, which leads to occupant discomfort and structural instability. To mitigate the excessive vibration in tall structures, tuned mass dampers (TMD), one of the oldest vibration absorbers, are used. They consist of a lumped mass connected to the structure by a spring and a viscous damper (Den Hartog, 1956). The TMD is designed in such a way that the natural frequency of the TMD coincides with the natural frequency of the superstructure, which results in resonance and hence energy due to external loads is dissipated. It is noticed that the performance of TMD relies on the mass of the TMD, i.e., a higher mass provides better energy dissipation. However, the larger mass may have an adverse effect on high-rise buildings. Also, the length of the viscous damper should be at least four times the stroke length.

In the recent past, inerters have gained popularity among researchers as an alternative to TMD, where the inertance of an inerter is significantly larger than its actual weight (Smith, 2002). It consists of flywheels that transform the linear displacement into rotational motion, by which the effective mass of the system is increased. Many variants of inerter have been proposed by researchers. Lazar *et al* (2014) proposed a tuned inerter damper which is connected to the structure by a spring and damper in series. A combination of inerter and TMD was proposed by Marian and Giaralis (2014) and showed the enhancement of energy dissipation under seismic events compared to the traditional TMD. Wen *et al* (2017) showed the effectiveness of multiple tuned inerter-based dampers using H_2 control theory. A rotational inertia double-tuned mass damper, which is an improved version of the tuned viscous mass damper, was proposed by Garrido *et al* (2013). Xie *et al* (2019) developed a cable-braced inerter system that is composed of a pair of bracing cables, a flywheel, and a shaft. When the structure experiences displacement, one of the cables is shortened by which shaft starts to rotate, and results the translational motion is transformed into rotational motion.

Despite the advantages of a tuned inerter damper (TID), few modifications are needed, such as the configuration of the TID. The TID consists of a spring, so that additional stiffness is added into the system, and hence the force demand on the member which is connected with the TID increases. In this view, a magnetic negative stiffness damper (MNSD) has been proposed in this study. The main advantage of this damper is that the additional stiffness is not added to the system. A few literatures are available on MNSD. Shi and Zhu (2015) proposed MNSD and the effectiveness of the damper was investigated by experimental simulation. Furthermore, they studied the design optimization of MNSD through parametric studies (Shi and Zhu, 2017). Liu and Lui (2020) proposed the mathematical expression for the nonlinear force-displacement hysteresis of MNSD, which was evaluated in the deterministic framework.

Energy harvesting has gained popularity in this decade where mechanical vibration energy of the controller can be transformed into electrical energy using an electromagnetic transducer. For energy harvesting, tuned inertial mass with an electromagnetic transducer was proposed by Asai *et al* (2018). Marian and Giaralis (2017) investigated the potential of energy harvesting using a tuned mass damper-inerter system for harmonically excited structures. Petrini *et al* (2020) proposed a tuned mass inerter damper with an electromagnetic transducer for wind-excited tall buildings. A back-driven ball screw mechanism combined with a rotary transducer was proposed by Cassidy *et al* (2011). Gonzalez-Buelga et al (2014) developed a combined system consisting of a tuned mass damper and an electromagnetic motor for mitigation of a structure's vibration and energy harvesting simultaneously. Tai and Zuo (2017) studied the optimal performance of the energy harvester for base-excited structures. Das et al (2021) investigated the optimal performance of a shape memory alloy based inerter system for simultaneous mitigation of wind induced vibration of tall structures and energy harvesting.

The literature presented above mainly focuses on the different advancements of inerter systems for the reduction of structural vibration due to earthquakes or winds and the potential for energy harvesting. This work investigated the performance of a modified inerter system which enables to reduce vibrational energy of the structure and converts it into electrical energy. With this in view, the following objectives are set for the present study-

- Develop an inerter system which combines a magnetic negative stiffness damper (MNSD) and an electromagnetic transducer. The purpose of using MNSD is that additional stiffness is not added into the system and also the nonlinear load-deformation hysteresis can absorb the vibrational energy.
- To produce the maximum electrical energy, a surrogate-assisted optimization has been carried out to reduce the computational burden. Kriging is used as a surrogate model.
- To establish the potential of the proposed control system for simultaneous vibration control and energy harvesting, a 76-storey building is being considered for numerical demonstration purposes.

2 Coupled Dynamics of Structure, Inerter and Energy Harvesting System

In this section, a high-rise benchmark building is used to demonstrate the proposed control system to mitigate the wind-induced vibration. The governing equations of motion and modeling details of the magnetic negative stiffness damper are elaborated in detail in the following subsections.

2.1 Governing Equations of Motion for Coupled System

Figure 1 illustrates the layout of the proposed control system, where an inerter is installed on the top floor of the building and the ineter is coupled with a magnetic negative stiffness damper (MNSD) for energy dissipation and an electromagnetic transducer for energy harvesting. In this proposed control system, the MNSD and the transducer are connected in parallel, whereas the entire system is connected with the inerter in series. The configuration of the inerter is shown in Figure 1(c), which consists of a rack, pinions, gears, and flywheels. The force induced by the inerter is expressed as

$$F_{in} = \frac{J_{in}}{r_{in}^2}\left(\ddot{x}_i - \ddot{x}_j\right) = M_{in}\ddot{x}_{in} \tag{1}$$

where J_{in} is the moment of inertia of the flywheel, r_{in} is the radius of the gear. x_{in} denotes the displacement of the inerter which is the relative displacement of two terminals (i.e., T1 and T2 in Figure 1(a)) of the inerter, i.e., $x_{in} = (x_i - x_j)$. Also, the over-dot in Eq. (1) shows the differentiation with respect to time. Therefore, the inertance of the inerter (M_{in}) equals to $\left(J_{in}/r_{in}^2\right)$.

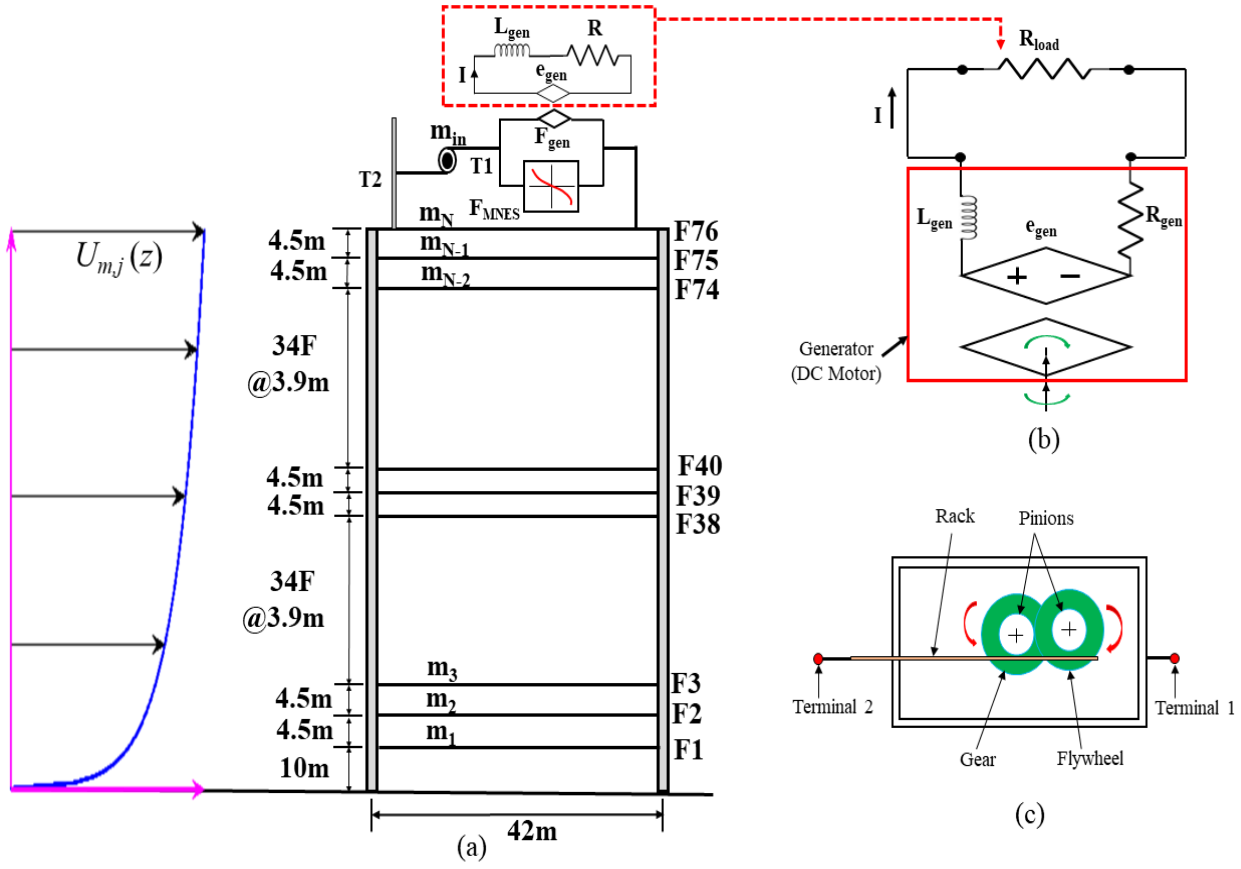

Figure 1: The architecture of the proposed control system; (a) Layout of 76-storey benchmark building, (b) Modeling of a DC motor connected with a resistor in series and (c) Configuration of inerter

The governing equations of motion of the coupled system subjected to wind loads (F_{wind}) can be written as

$$M\ddot{x} + C\dot{x} + Kx - F_{MNSD} + K_f I = F_{wind} \tag{2}$$

$$M_{in}\ddot{x}_{in} + F_{MNSD} - K_f I = 0 \tag{3}$$

$$K_v\left(\dot{x}_{in} - \dot{x}_N\right) + RI + L_{gen}\dot{I} = 0 \tag{4}$$

where M, C, and K are the mass, damping, and stiffness matrices of the primary structure, respectively. x is a vector of floor displacement, i.e., $x = [x_1, x_2, \ldots, x_N]^T$, where N is the total number of floors in the primary structure. F_{MNSD} in Eq. (2) represents the force induced by the magnetic negative stiffness damper, whose details are provided in the following subsection. Also, in Eq. (3), R denotes the resistance of the electromagnetic transducer, which is equivalent to $R = (R_{gen} + R_{load})$, where R_{gen} and R_{load} are the resistance of the generator and the external resistance, respectively. The inductance of the generator is denoted by L_{gen}. According to Faraday's law of electromagnetic induction, when the generator is attached to a rotating mechanical system, the electromotive force (EMF) induced in the generator, i.e., e_{gen} is proportional to the relative angular velocity of the mechanical system $\left(\dot{\theta}_{gen}\right)$, which is expressed as

$$e_{gen}(t) = K_v\dot{\theta}_{gen}(t) \tag{5}$$

where K_v is the motor's back-EMF constant. Also, from Lorentz's force law, the torque produced in the mechanical system depends on the electric current (I) induced in the coil of the generator, which is given by

$$\tau_{gen}(t) = K_f I(t) \tag{6}$$

where K_f is the motor torque constant. From Eq. (5) and Eq. (6), the relation between torque and the angular velocity of the generator can be expressed as (Lin *et al*, 2021)

$$\tau_{gen}(t) = \frac{K_v K_f}{R_{gen} + R_{load}}\dot{\theta}_{gen}(t) \tag{7}$$

The power generated by the electromagnetic transducer is expressed as

$$P_g(t) = I^2(t)R_{load} \tag{8}$$

2.2 Modeling Details of Magnetic Negative Stiffness Damper

In this study, a magnetic negative stiffness damper (MNSD) is used as a passive vibration absorber, as proposed by Shi and Zhu (2015). As shown in Figure 2, the MNSD consists of three magnets placed in a non-ferromagnetic (e.g., copper) conductive pipe. One of these is movable. Two magnets are stationary at opposite ends of the conductive pipe. When the structure experiences displacement due to external dynamic loads, the movable magnet is displaced from the equilibrium position. To maintain the equilibrium position of the movable magnets, an opposite force is exerted by one of the stationary magnets, which is opposite to the motion of the movable magnet. Thus, negative stiffness is experienced. Also, as the conductive pipe is made of non-ferromagnetic material, an eddy current is induced due to the change in magnetic flux when the magnet is moving, thus damping is induced in the system. There are different phenomenological models available to define the load–deformation hysteresis of the MNSD. In this study, Liu and Lui (2020) is used to represent the nonlinear hysteresis of the MNSD, which is derived within the deterministic framework. The force exerted by the MNSD is expressed as

$$F_{MNSD} = C_{MNSD}\dot{x}_{in} \tag{9}$$

where the damping coefficient, C_{MNSD} is written as

$$C_{MNSD} = M_0^2\mu_0^2R^3\sigma\varepsilon\left[\frac{a}{1+\left(\frac{\varepsilon}{b}\right)^c}\right] \tag{10}$$

where M_0 is the magnetization, μ_0 is the magnetic constant, and σ is the conductivity of the pipe. In the above equation, R denotes the magnetic radius and $\varepsilon = (R_2 - R_1)/R_1$, where R_1 and R_2 are the inner and outer radii of the conductive pipe. The constants a, b, and c are expressed as follows

$$a = -\theta_1\zeta^2 + \theta_2\zeta + \theta_3 \tag{11}$$

$$b = -\theta_4\zeta^2 + \theta_5\zeta + \theta_6 \tag{12}$$

$$c = -\theta_7\zeta^2 - \theta_8\zeta + \theta_9 \tag{13}$$

where ζ is the aspect ratio of the magnet. In the above equations, the constants $\theta_1,...,\theta_9$ depend on the manufacturing process, which helps the designer to tune the MNSD against the stochastic loads.

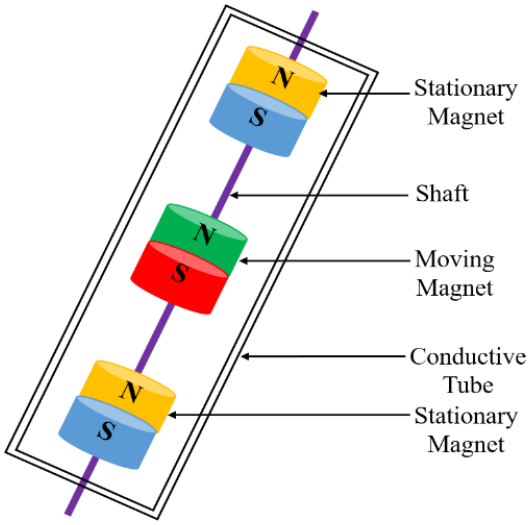

Figure 2: The architecture of the proposed control system

3 Simulation of Stochastic Wind Loads

In this study, the wind loads are simulated for the along-direction of the building floors, which are assumed to be quasi-steady. It has two components, i.e., mean and fluctuating components. The wind force acting on the *i*-th floor is expressed as

$$W_i = \frac{1}{2}\rho C_D A_i\left[U_{m,i}(t) + U_{f,i}(t)\right]^2\lambda_D(f) \approx \rho C_D A_i U_{m,i}(t)U_{f,i}(t) \tag{14}$$

In the above equation, ρ is the air density, C_D is the drag coefficient, which depends on the shape of the building, and A_i is the projected frontal area of the building perpendicular to the wind flow. The mean and fluctuating components of the wind velocity at the *i*-th floor of the building are represented by $U_{m,i}$ and $U_{f,i}$.

In Eq. (14), λ_D is the aerodynamic admittance for drag, which depends on the frequency (f) and equals 1.0 for quasi-static conditions. The mean component of the wind velocity, $U_{m,i}(t)$, at the *i*-th floor of the building is expressed using the logarithmic law (Simiu and Scanlan, 1996), given by

$$U_{m,i}(z) = U_m(z_{10}) \frac{\ln(z/z_0)}{\ln(10/z_0)} \tag{15}$$

where z is the height measured from ground level, $U_m(z_{10})$ is the mean wind velocity at z = 10m, and z_0 is the terrain roughness length. In Eq. (14), the fluctuating component of the wind velocity, $U_{f,i}$ is estimated using the spectral method, proposed by Shinozuka and Deodatis (1991). The power spectral density matrix for the stochastic wind field of a *N*-storeys building is written as

$$S(\omega) = \begin{bmatrix} S_{11}(\omega) & \cdots & S_{1N}(\omega) \\ \vdots & \ddots & \vdots \\ S_{N1}(\omega) & \cdots & S_{NN}(\omega) \end{bmatrix} \tag{16}$$

where ω is the frequency in rad/sec. The elements of S(ω) in Eq. (16), i.e., $S_{ij}(\omega)$ is expressed as

$$S_{ij}(\omega) = \begin{cases} S_i(\omega), & \text{if} \quad i = j \\ \sqrt{S_i(\omega) S_j(\omega)}\,\psi_{ij}(\omega), & \text{if} \quad i \neq j \end{cases} \tag{17}$$

where $S_i(\omega)$ denotes the power spectral density function (PSDF) and $\psi_{ij}(\omega)$ is the coherence function between the turbulence between the *i*-th floor and the *j*-th floor, corresponding to z_i and z_j heights, respectively. The coherence function, $\psi_{ij}(\omega)$ is given by

$$\psi_{ij}(\omega) = \exp\left[-\frac{\omega}{2\pi} \frac{C_z |z_i - z_j|}{0.5(U_{m,i} + U_{m,j})} \right] \tag{18}$$

where C_z is the correlation coefficient. The power spectral density function, S(ω) in Eq. (16), is decomposed using Cholesky decomposition and is expressed as

$$S(\omega) = L(\omega) L^{T*}(\omega) \tag{19}$$

In the above equation, L(ω) is the lower triangular matrix for every ω whose complex conjugate is denoted by $L^*(\omega)$. The matrix L(ω) is expressed as follows

$$L(\omega) = \begin{bmatrix} L_{11}(\omega) & \cdots & 0 \\ \vdots & \ddots & \vdots \\ L_{N1}(\omega) & \cdots & L_{NN}(\omega) \end{bmatrix} \tag{20}$$

In this study, fluctuating component of the wind velocity are modelled as a stationary process, where the standard deviation of the fluctuating wind velocity is independent of time. The Davenport spectrum is used to simulate the stationary fluctuating wind speed, which is expressed as

$$S_i(\omega) = \frac{\left[\sigma^S(z)\right]^2}{6}\frac{2\pi}{\omega}\frac{4P^2}{\left(1+P^2\right)^{4/3}} = \frac{1}{2}\frac{u_*^2}{\omega}\frac{4P^2}{\left(1+P^2\right)^{4/3}} \tag{21}$$

where $P = \frac{1200\omega}{2\pi U_m(z_{10})}$ and the wind shear (u_*) in the above equation is written in the following form

$$u_* = \frac{k_0 U_{m,i}(z)}{\ln(z/z_0)} \tag{22}$$

where k_0 is the von-Karman constant, which is assumed to be 0.4 in this study. Once the PSDF for the stationary process is defined, the fluctuating wind velocity time history $U_{f,i}$ at the *i*-th floor of the building is simulated by using the superposition of trigonometric functions with random phase angles, which is expressed as

$$U_{f,i}^S(t) = 2\sum_{m=1}^{N}\sum_{l=1}^{N_\omega}\left|L_{im}(\omega_{ml})\right|\sqrt{\Delta\omega}\cos\left[\omega_{ml}t - \theta_{ml}(\omega_{ml}) + \Phi_{ml}\right] \tag{23}$$

where L_{im} is the element of the matrix $L(\omega)$ defined in Eq. (20). Also, $\Delta\omega$ is the frequency step, which is equal to (ω_u/N_ω). The cut-off frequency is denoted by ω_u and N_ω is the total number of divisions in the frequency scale which is equal to $\omega_{ml} = l\Delta\omega - \left(\frac{m-l}{m}\right)\Delta\omega$. In Eq. (23), Φ_{ml} is the random phase angle which is uniformly distributed between 0 and 2π. Also, $\theta_{ml}(\omega_{ml}) = \tan^{-1}\left\{\frac{\mathrm{Im}\left[L_{im}(\omega_{ml})\right]}{\mathrm{Re}\left[L_{im}(\omega_{ml})\right]}\right\}$, where Im[.] and Re[.] are the imaginary and real components, respectively.

4 Reliability based Optimal Tuning of Proposed Control System

The nonlinear model of the combined structural system coupled with the magnetic negative stiffness damper based inerter system is elaborated in the previous section, which is exposed to stochastic wind loads. The purpose of the proposed control system is to maximize energy harvesting. Thus, the optimization of the proposed control system is needed to ensure the maximum power generated. Monte Carlo simulation is one of the oldest and most robust method for optimization. In reality, this method is not suitable for high-fidelity models where many samples are required to capture the nonlinearity of the structural system, and thus, it becomes computationally expensive. To reduce the computational cost, surrogate assisted optimization has gained popularity in recent decades. In this study, Kriging, a well-known surrogate model, is used, whose details are provided in the following subsection.

4.1 Kriging Surrogate Model

Kriging is a stochastic modelling technique that produces the probabilistic responses from data samples using an interpolation scheme by minimizing the mean squared error. It approximates the original response surface with the assumption that the output from the Kriging is evaluated by a Gaussian process whose mean and autocorrelation are unknown and computed from the training dataset. The output response, which is a function of input design variables, is expressed as follows

$$Y \approx \sum_{i=1}^{m}\eta_i f_i(X) + \psi(X) = f(X)^T\eta + \psi(X) \tag{24}$$

where X is the vector of design variables, f(X) is the vector of m numbers of known regression functions, and η is the regression coefficient vector. Also, in the above equation, ψ(X) is the error function, which is assumed to be a stationary Gaussian process with a zero mean, constant variance σ^2 and the auto-correlation function Q. The autocovariance function of ψ(X) is expressed as follows

$$E\left[\psi(X_i)\psi(X_j)\right] = \sigma^2 Q(X_i, X_j; \theta) \tag{25}$$

where E[.] is the expectation operator and $Q(X_i,X_j;\theta)$ is the correlation between the samples X_i and X_j with respect to hyperparameter θ. In this study, the Gaussian correlation function is used, which is written as

$$Q(X_i, X_j; \theta) = \prod_{k=1}^{m} \exp\left\{-\theta_k \left(X_{i,k} - X_{j,k}\right)^2\right\} \tag{26}$$

where $X_{i,k}$ and $X_{j,k}$ are the k-th components of X_i and X_j, respectively. The hyperparameter θ is estimated using a maximum likelihood estimate. Also, the regression coefficient η in Eq. (24) is estimated by the least-square method. The details of the entire procedure of Kriging are found in Das *et al* (2021).

4.2 Optimization of the Proposed Control System

In this study, Kriging is adopted for reliability-based optimization of the combined inerter system. The tuning parameters of the proposed control system are designed so that maximum power can be generated. In this case, the uncertainty is associated with the wind loads. The performance function for the optimization is considered as follows

$$\beta = \frac{\mu_{Pg}}{\sigma_{Pg}} \tag{27}$$

where β is the reliability index, which is a ratio of the mean (μ_{Pg}) and standard deviation (σ_{Pg}) of the maximum value of power generated from an ensemble of wind load time histories. Within this view, the RBDO problem is formulated as

$$\begin{aligned} X^* &= \arg\max_X \left[\beta(X, \kappa)\right] \\ \text{s.t.} X_{LL} &\le X \le X_{UL} \end{aligned} \tag{28}$$

where $X = [R, \zeta, R_1, R_2, \theta_1, \ldots, \theta_9]$ are the design variables which are bounded by lower and upper limits, X_{LL} and X_{UL}, respectively. R and ζ are the radius and aspect ratio of the magnet. R_1 and R_2 are the inner and outer radii of the conductive pipe, and $\theta_1, \ldots, \theta_9$ are parameters which control the hysteresis of the MNSD, as defined in Eq. (11) - Eq. (13). In Eq. (28), κ is the uncertainty related to the wind loads. The entire framework of the optimization is shown in Figure 3.

5 Numerical Results

In this study, a 76-storeys high-rise benchmark building is taken (Yang et al., 2004) for demonstration purposes. The building is located in Melbourne, Australia. It was made of reinforced concrete, consisting of a concrete core and a concrete frame. The total height of the structure is 306m, where the first storey is 10m high from ground level, the storey heights for the 2nd and 3rd floors, 38th to 40th, and 74th to 76th, are 4.5m, and the other storey heights are 3.9m, as shown in Figure 1. The total mass of the structure is 153,000 metric tons, including heavy machinery in plant rooms. The aspect ratio (i.e., the height to width ratio) is 7.3, which means the structure is slender and highly sensitive to wind-induced vibration. The core of the structure is designed to resist the wind loads and the gravitational loads and part of wind loads are carried by concrete frames. In this study, all rotational degrees of freedom are eliminated by using a static

condensation procedure, and only translational degrees of freedom are considered, i.e., one for each floor. The natural frequencies of the building are found to be 0.16, 0.765, and 1.992 Hz. The damping ratio is 1% in all modes following Rayleigh's model. Figure 4 shows the first three modal frequencies and mode shapes of the benchmark building.

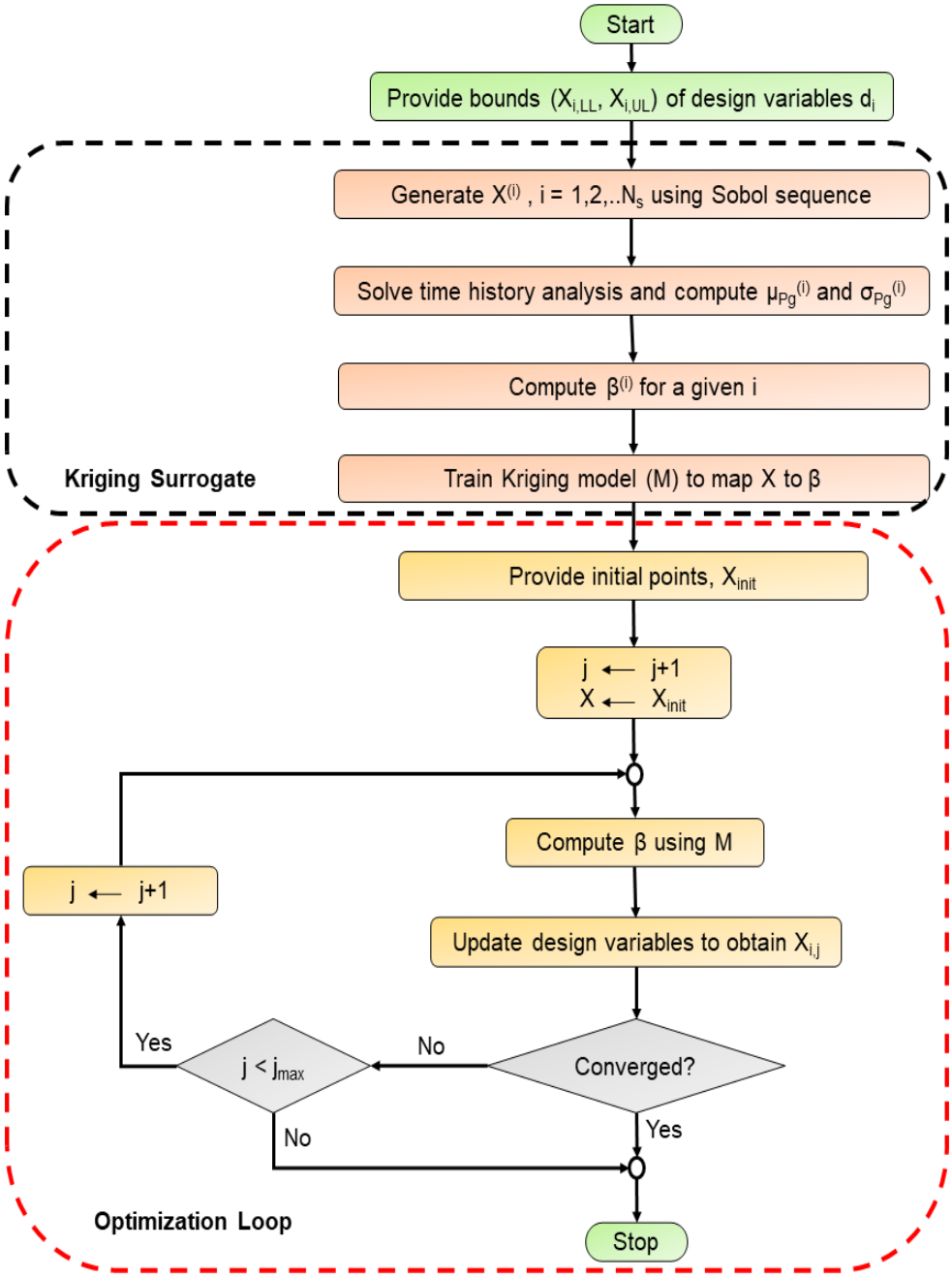

Figure 3: Flowchart representing Kriging based RBDO

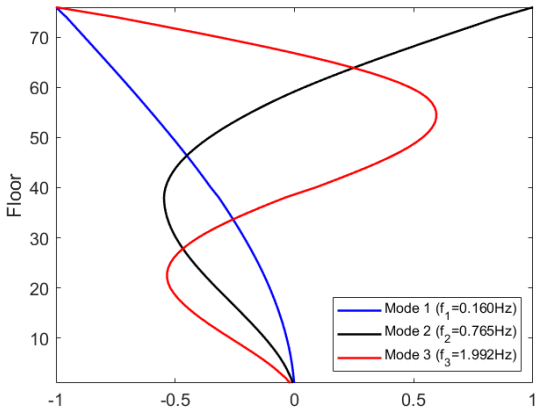

Figure 4: Mode shape and modal frequencies of 76-storey benchmark building

Once the structural properties are defined, the wind loads are estimated for different floors of the building using the quasi-steady model, described in Section 3. The air density (ρ) is assumed to be 1.226 kg/m^3. The random wind loads have mean and fluctuating components, where the mean component of the wind loads at every floor is computed using the logarithmic power law and the stationary fluctuating part is simulated using the Davenport spectrum. The mean wind speed at 10m above ground level is assumed to be 25 m/s. The ground roughness coefficient is assumed to be 0.3. Figure 5 shows the wind velocity acting on different floors of the building considering stationary fluctuating components. Also wind force time history for two cases at 70th and 76th floors are shown in Figure 6(a) and Figure 6(b), respectively. Figure 6(c) depicts the auto power spectral density function (PSDF) at the 76th floor. Similarly, Figure 6(d) illustrates the cross PSDF between 70th and 76th floors. It is seen that the target PSDF and the ensemble average of PSDF of fluctuating components of stationary wind loads simulated from the target PSDF match well.

Once the wind loads are simulated, attention is focused on the reliability-based optimization of the proposed controller, which is achieved by the tuning of the parameters of the proposed controller. The wind loads are assumed to be the only source of the uncertainty. The mean value of design parameters are taken: μ_R (radius of the magnet) = 10mm, aspect ratio (ζ) of the magnet = [0.05, 2], μ_{R1} (inner radius of the conductive pipe) = 11mm, μ_{R2} (outer radius of the conductive pipe) = 17mm, the constants related to the hysteresis of the MNSD, [$\mu_{\theta 1}$,…,$\mu_{\theta 9}$] = [0.39 ,1.213, 0.19, 0.1375, 0.5043, 0.14, 0.033, 0.006, 1.1146]. The mean value is denoted by μ in the above. All the design variables are assumed to be uniformly distributed with coefficient of variation of 20%. As Kriging is the approximate model which predicts the output responses based on few observations called Design of Experiment (DoE). Therefore, attention is devoted to the accuracy of the surrogate model. Different sizes of DoE set, i.e., from 75 to 200 samples with an increment of 25 samples, are considered, which are generated using the Sobol sequence. With the DoE samples, a Kriging model is trained, and 50,000 prediction points of design variables are passed through the trained Kriging model to obtain the predicted outputs. The same prediction points are used for estimating the accuracy. Figure 7 shows the convergence history for different sizes of the DoE set. It is seen that a minimum of 125 DoE samples are needed in this case. With this DoE set, the optimization is carried out. The optimum design parameters are obtained as: R = 9.6mm, ζ = 1.99, R_1 = 10.8mm, R_2 = 13.6mm, the constants related to the hysteresis of the MNSD, [θ_1,…, θ_9] = [0.51 ,1.06, 0.25, 0.16, 0.39, 0.11, 0.04, 0.0074, 0.898].

With the optimized design parameters, time history analysis is performed. Figure 8 shows the top floor displacement time history without and with controller. It is seen that the peak displacement of the top floor is reduced by 56% while using the proposed controller. The rms reduction is found to be 49%. Besides the reduction of peak and rms displacement of the top floor, the generated power time history is shown in Figure 9(a). It is seen that the maximum power generated is found to be 716W. Also, the ensemble average of power generated using the proposed control strategy is shown in Figure 9(b).

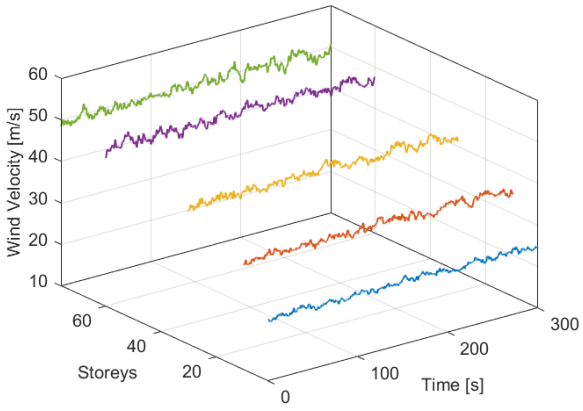

Figure 5: Wind velocity time histories at different floors considering stationary fluctuating component

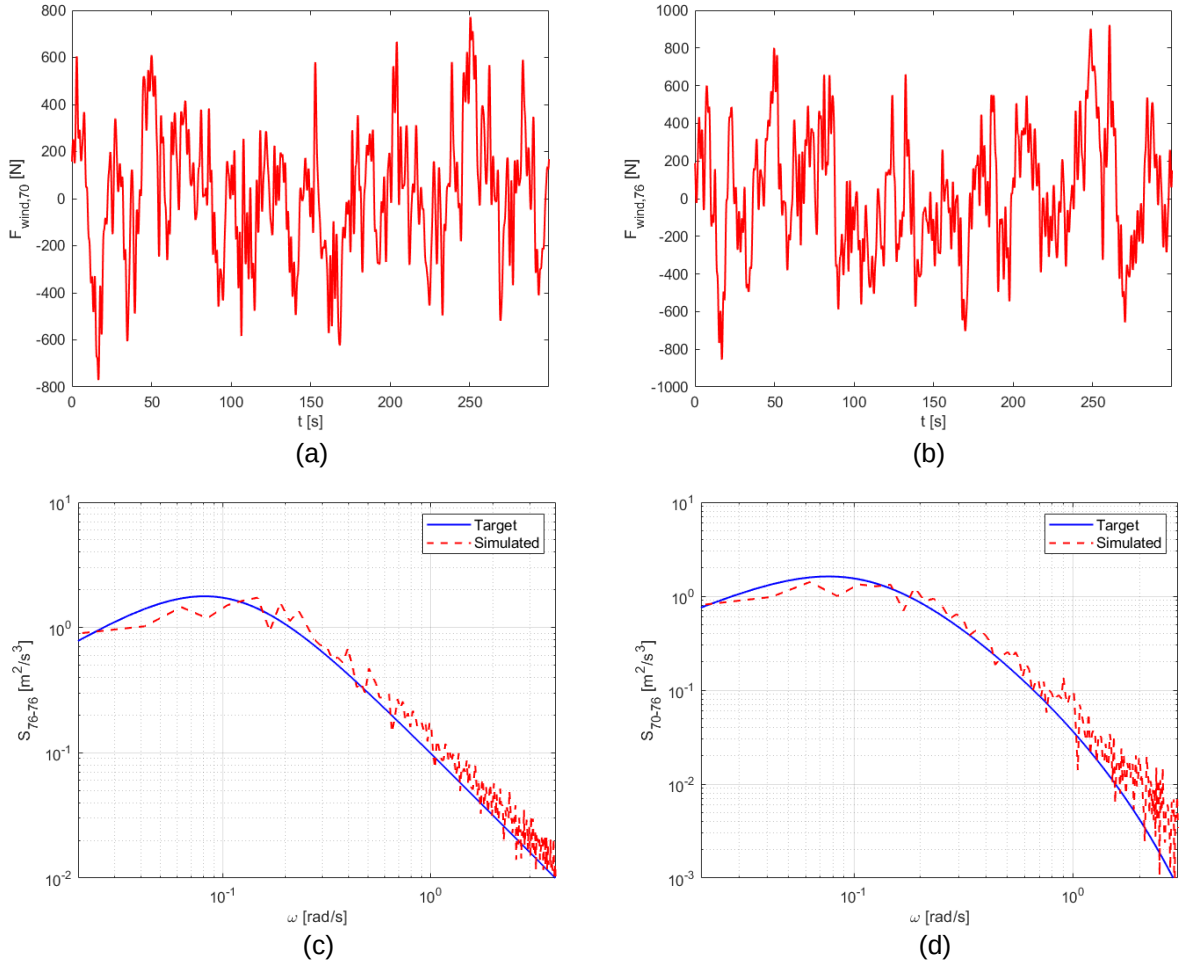

Figure 6: Wind force simulation; (a) time history at 70th floor, (b) time history at 76th floor, (c) auto PSDF at 76th floor and (c) cross PSDF between 70th and 76th floor

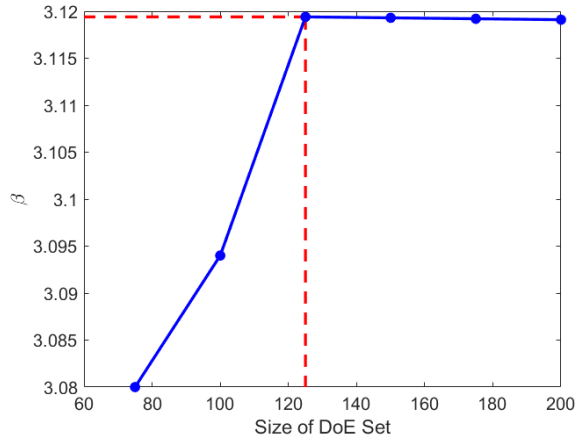

Figure 7: Convergence history for different sizes of DOE sets

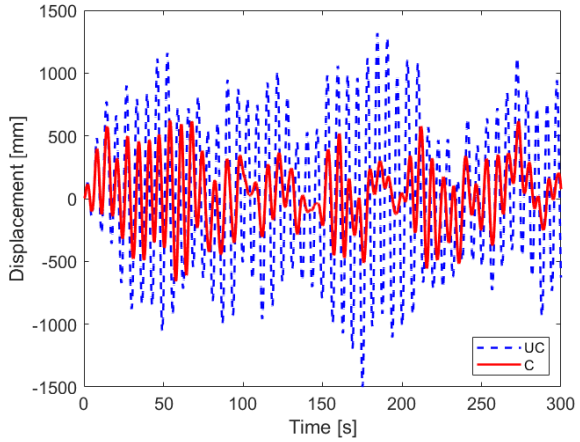

Figure 8: Top floor displacement without and with controller for stationary winds

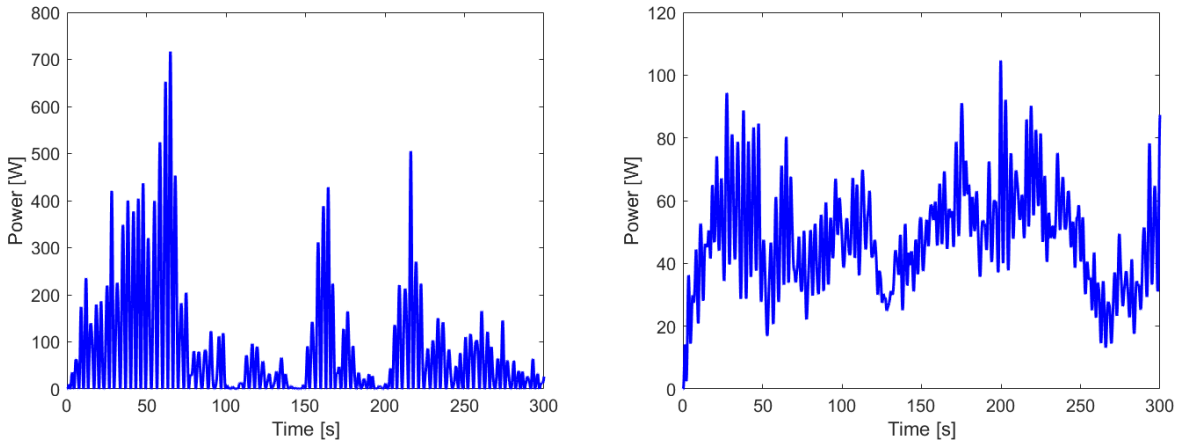

(a) (b)

Figure 9: (a) Power generated for single wind load time history and (b) Ensemble average of power generated

6 Conclusions

The theoretical study presented in this paper is focused on the performance of the magnetic negative stiffness damper based inerter system for mitigating the wind induced vibration of tall structures. It also investigates the potential of energy harvesting using the proposed control system. The major contributions of the present study are listed below-

- The numerical results presented in the previous section establish the effectiveness of the proposed control system for mitigating the wind-induced vibration of the structure and energy harvesting, i.e., the conversion of vibrational energy into electrical energy. It shows the effectiveness of the proposed control system in terms of reducing the peak and rms values of the floor displacement.
- To generate the maximum power, the parameters associated with the proposed control system are tuned using stochastic optimization. Kriging is used as a surrogate model for optimization. It is seen that the optimization technique is very efficient at reducing the computational cost while operating in a stochastic environment.

All these aspects clearly indicate the effectiveness of the proposed control system for reducing the wind induced vibration of high-rise buildings, and the dissipated energy is converted into power.

Acknowledgements

The authors acknowledge the financial support through Natural Sciences and Engineering Research Council of Canada Discovery Grants Program (RGPIN-2019-05584).

References

Asai, T., Araki, Y. and Ikago, K. 2018. Structural control with tuned inertial mass electromagnetic transducers. *Structural Control and Health Monitoring*, **25**(2): e2059.

Cassidy, I. L., Scruggs, J. T., Behrens, S. and Gavin, H. P. 2011. Design and experimental characterization of an electromagnetic transducer for large-scale vibratory energy harvesting applications. *Journal of Intelligent Material Systems and Structures*, **22**(17): 2009-2024.

Das, S., Chakraborty, A. and Barua, I. 2021. Optimal tuning of SMA inerter for simultaneous wind induced vibration control of high-rise building and energy harvesting. *Smart Materials and Structures*, **30**(2): 025027.

Den Hartog, J. P. 1956. Mechanical Vibrations. 4th edn (New York: McGraw-Hill).

Garrido, H., Curadelli, O. and Ambrosini, D. 2013. Improvement of tuned mass damper by using rotational inertia through tuned viscous mass damper. *Engineering Structures*, **56**: 2149-2153.

Gonzalez-Buelga, A., Clare, L. R., Cammarano, A., Neild, S. A., Burrow, S. G. and Inman, D. J. 2014. An optimised tuned mass damper/harvester device. *Structural Control and Health Monitoring*, **21**(8): 1154-1169.

Hong, H.P. 2016. Modeling of nonstationary winds and its applications. *Journal of Engineering Mechanics*, **142**(4): 04016004.

Lazar, I. F., Neild, S. A. and Wagg, D. J. 2014. Using an inerter-based device for structural vibration suppression. *Earthquake Engineering & Structural Dynamics*, **43**(8): 1129-1147.

Lin, G. L., Lin, C. C., Chen, Y. J. and Hung, T. C. 2021. Experimental verification of electromagnetic multiple tuned mass dampers for energy harvesting and structural control. *Earthquake Engineering & Structural Dynamics*, **50**(13): 3483-3504.

Liu, W. and Lui, E. M. 2020. Mathematical modeling and parametric study of magnetic negative stiffness dampers. *Advances in Structural Engineering*, **23**(8): 1702-1714.

Marian, L. and Giaralis, A. 2014. Optimal design of a novel tuned mass-damper–inerter (TMDI) passive vibration control configuration for stochastically support-excited structural systems. *Probabilistic Engineering Mechanics*, **38**: 156-164.

Marian, L. and Giaralis, A. 2017. The tuned mass-damper-inerter for harmonic vibrations suppression, attached mass reduction, and energy harvesting. *Smart Structures and Systems*, **19**(6): 665-678.

Petrini, F., Giaralis, A. and Wang, Z. 2020. Optimal tuned mass-damper-inerter (TMDI) design in wind-excited tall buildings for occupants' comfort serviceability performance and energy harvesting. *Engineering Structures*, **204**: 109904.
Shi, X. and Zhu, S. 2015. Magnetic negative stiffness dampers. *Smart Materials and Structures*, **24**(7): 072002.
Shi, X. and Zhu, S. 2017. Simulation and optimization of magnetic negative stiffness dampers. *Sensors and Actuators A: Physical*, **259**: 14-33.
Shinozuka, M. and Deodatis, G. 1991. Simulation of stochastic processes by spectral representation. *Applied Mechanics Reviews*, **4**(44): 191-204.
Simiu, E. and Scanlan, R.H. 1996. Wind Effects on Structures: Fundamentals and Applications to Design (Vol. 688). New York: John Wiley.
Smith, M. C. (2002). Synthesis of Mechanical Networks: the Inerter. *IEEE Transactions on Automatic Control*, **47**(10): 1648-1662.
Tai, W. C. and Zuo, L. 2017. On optimization of energy harvesting from base-excited vibration. *Journal of Sound and Vibration*, **411**: 47-59.
Wen, Y., Chen, Z. and Hua, X. 2017. Design and evaluation of tuned inerter-based dampers for the seismic control of MDOF structures. *Journal of Structural Engineering*, **143**(4): 04016207.
Xie, L., Ban, X., Xue, S., Ikago, K., Kang, J. and Tang, H. 2019. Theoretical study on a cable-bracing inerter system for seismic mitigation. *Applied Sciences*, **9**(19): 4096.
Yang, J.N., Agrawal, A.K., Samali, B. and Wu, J.C. 2004. Benchmark problem for response control of wind-excited tall buildings. *Journal of Engineering Mechanics*, **130**(4): 437-446.